Chemical Engineering Journal 148 (2009) 173–183

Contents lists available at ScienceDirect

Chemical Engineering Journal

journal homepage: www.elsevier.com/locate/cej

Modelling transport phenomena and chemical reactions in automotive three-way catalytic converters

H. Santos [a], M. Costa [b,*]

[a] Mechanical Engineering Department, School of Technology and Management, Polytechnic Institute of Leiria, Morro do Lena – Alto Vieiro Apt. 4163, 2411-901 Leiria, Portugal
[b] Mechanical Engineering Department, Instituto Superior Técnico, Technical University of Lisbon, Avenida Rovisco Pais, 1049-001 Lisbon, Portugal

ARTICLE INFO

Article history:
Received 4 June 2008
Received in revised form
27 November 2008
Accepted 30 November 2008

Keywords:
Mathematical modelling
Transport processes
Multiphase reactions
Three-way catalyst
Monolith structures
Washcoat structures
Conversion

ABSTRACT

This study concentrates on the external and internal mass transfer with multiple reactions in the catalytic layer of a three-way catalyst (TWC). A single channel model accounting for the species diffusion inside the washcoat using the effectiveness factor was developed. Validation and calibration of the model was achieved by comparing predictions against experimental data obtained previously by the same authors. The model was then applied to study the importance of both turbulent monolith structures and controlled washcoat structures on TWC conversions. The numerical results show that: (i) increasing the transport coefficients using turbulent monolith structures can produce either positive or negative effects on the TWC conversions; (ii) overall, the net effect of increasing the transport coefficients on the TWC conversions is positive; (iii) at high inlet gas temperatures and high space velocities the turbulent monolith structures present important improvements in the TWC conversions; (iv) the TWC conversions can be significantly improved enhancing the transport properties of the porous washcoat structure; (v) enhancements in the transport properties of the washcoat structure have deeper impacts on the TWC conversions than improvements in the monolith channel structure.

1. Introduction

Automotive emission standards are becoming increasingly stringent which requires continuous improvements in the exhaust after treatment systems. Since the cold start emissions may represent more than 50% of the total emissions, most studies available in the literature have concentrated on improving the light-off behavior. As a consequence of this intense research and development, today the three-way catalyst (TWC) reach the light-off temperature very rapidly and, thus, the relative importance of the emissions above light-off is becoming gradually more important. In order to achieve future emission standards (*e.g.*, US 2010 and EURO VI), conversions very close to 100% have to be achieved under warmed up conditions.

Several authors (*e.g.*, [1–4]) have demonstrated that both internal and external mass transfer resistances limit the TWC conversions above light-off temperature. Thus, the diffusion resistances in the boundary layer (external mass transfer) and in the washcoat (internal mass transfer) have to be as low as possible to achieve high conversions.

The diffusion and reaction within the washcoat can be accounted for using: (a) a detailed three-dimensional (3D) model of the porous washcoat [4], (b) a model of the pseudo-homogeneous washcoat layer with explicit solution of one dimensional (1D) internal diffusion in the transverse direction [5], and (c) a model of the washcoat layer with diffusion effects lumped into the effectiveness factor. Zygourakis and Aris [5] and Wanker et al. [6] showed that the use of the effectiveness factor model is adequate for temperatures above the light-off temperature and for low concentrations of reactants, as those encountered in exhaust aftertreatment systems such as TWC. A detailed discussion on the validity of the effectiveness factor model is presented in Appendix A.

Massing et al. [3] used the 1D plug-flow model (PFM) with the effectiveness factor and provided a comparison between measurements and predictions. To promote simplicity, they studied TWC conversions under steady-state conditions solely for propene oxidation. In the present study, TWC conversions were also studied under steady-state conditions, but the model has been extended to account for the conversion of the three main chemical species (CO, unburnt hydrocarbons – HC – and NO_x). Here we have also used the 1D PFM with the effectiveness factor implemented. The model was calibrated and validated through comparisons against our previous measurements [7]. Subsequently, the model was applied to study the importance of both turbulent monolith structures and controlled washcoat structures on TWC conversions.

In the last few years the improvements of the TWC conversions above light-off temperature were achieved through advances on

* Corresponding author. Tel.: +351 218417378; fax: +351 218475545.
E-mail address: mcosta@ist.utl.pt (M. Costa).

1385-8947/$ – see front matter © 2008 Elsevier B.V. All rights reserved.
doi:10.1016/j.cej.2008.11.047

Nomenclature

$a_{j,k}$	stoichiometric coefficient of specie j in reaction k
A	pre-exponential Arrhenius factor (mol K m^{-3} s^{-1})
c_{pg}	gas specific heat capacity (J kg^{-1} K^{-1})
c_{ps}	solid specific heat capacity (J kg^{-1} K^{-1})
C_g	mean concentration in the gas phase, mole fraction
C_{ref}	reference concentration in the solid phase, $C_{\text{ref}} = C_s(\rho_g/M_g)$ (mol m^{-3})
C_s	mean concentration in the solid phase, mole fraction
d_p	mean pore diameter (m)
D	combination of bulk and Knudsen diffusion (m^2 s^{-1})
D_b	bulk diffusion (m^2 s^{-1})
D_{eff}	effective diffusion (m^2 s^{-1})
D_K	Knudsen diffusion (m^2 s^{-1})
E_a	activation energy (J mol^{-1})
ΔF	elementary exchange area (m^2)
h	heat transfer coefficient (W m^{-2} K^{-1})
ΔH	enthalpy of the reaction (J mol^{-1})
ΔHa	adsorption enthalpy of the reaction (J mol^{-1})
k_m	mass transfer coefficient from the bulk gas to the washcoat surface (m s^{-1})
k_s	solid phase conductivity (W m^{-1} K^{-1})
k_V	reaction rate constant based on washcoat volume (s^{-1})
$\dot{m}_g$	mass flow rate (kg s^{-1})
M	molecular weight (kg mol^{-1})
M_g	molecular weight of the exhaust gases (kg mol^{-1})
$\dot{n}$	molecular flux (mol m^{-3} s^{-1})
$NTUh$	number of transfer units for heat
$NTUm$	number of transfer units for mass
Nu	Nusselt number
$Nu_{T,\infty}$	asymptotic Nusselt number for constant wall temperature
Pr	Prandtl number
r_k	reaction rate (mol m^{-3} s^{-1})
R_Ω	effective transverse diffusion length (m)
R_E	external mass transfer resistance
R_G	global (total) mass transfer resistance
R_L	internal mass transfer resistance
R	species rate, expressed per channel volume (mol m^{-3} s^{-1})
R_P	particular gas constant (J kg^{-1} K^{-1})
r_k	reaction rate (mol m^{-3} s^{-1})
S	mass transfer area per unit of catalyst volume (m^{-1})
Sc	Schmidt number
Sh	Sherwood number
$Sh_{T,\infty}$	asymptotic Sherwood number for constant wall temperature
Δt	time step (s)
T_g	mean temperature in the gas phase (K)
T_s	mean temperature in the solid phase (K)
u_z	flow velocity in the longitudinal direction (m s^{-1})
V_{macro}	macro pore volume (m^3)
V_{meso}	meso pore volume (m^3)
V_{total}	total pore volume (m^3)
ΔV	elementary reactor volume (m^3)
X	fractional conversion
z	axial length (m)
ΔZ	elementary axial grid length (m)

Greek letters

α_g	gas thermal diffusivity (m^2 s^{-1})
α_s	solid thermal diffusivity (m^2 s^{-1})
δ_C	effective washcoat thickness (m)
ε	void fraction
ε_p	porosity
η_L	local effectiveness factor
μ_g	gas dynamic viscosity (N s m^{-2})
ν_g	kinematic viscosity of the exhaust gas mixture (m^2 s^{-1})
ρ_g	gas mass density (kg m^{-3})
ρ_s	solid mass density (kg m^{-3})
τ	pore tortuosity factor
ϕ_L	washcoat Thiele modulus

Sub- and superscripts

amb	ambient
E	external
g	gas
G	global
i	space node index
in	at channel inlet
j	indication of exhaust species
k	indication of reaction k
L	local (internal, within the washcoat)
m	mass
n	temporal index
N	total number of gas phase species
s	solid
z	axial coordinate

the external mass transfer of the monolith structures. To this end, for example, both metallic and ceramic straight channel monoliths with cell densities from 400 cpsi up to 1200 cpsi along with thin foils have been introduced [8]. In spite of these reactors providing larger geometrical surface areas, the TWC still operates within the laminar flow region which limits the external mass transport process.

The external mass transfer limitation of the laminar flow through monoliths can be overcome by using the so-called turbulent monoliths [9,10]. These innovative monolith structures can operate in the transition or turbulent regions because they usually have a small diameter and are constructed with protrusions in the channel walls in order to enhance the radial transport within the TWC channels. Thus, with these monolith structures, the external transport phenomenon is significantly enhanced as compared with the straight channels.

The internal mass transfer limitation on the TWC conversions can be reduced by favoring the accessibility of the reactants towards the active sites located within the washcoat structure. In this respect, an enormous progress has recently been made in the field of ordered porous structured materials. Studies concerning the synthesis of materials with controlled micro–meso–macro pore structure, zeolites type or metal oxides such as alumina, silica, titania or zirconia are now available in the literature (*e.g.*, [11,12]). Given these recent advances in the washcoat structures, it is important to study its performance when applied to TWC, as it is done in the present study.

2. Mathematical model

2.1. Model description

The most important simplification encountered in the modelling approaches available in the literature is the representation of the whole matrix (thousands of channels) by a single channel with the

assumption of equivalent passages with no interaction. The single channel modelling (SCM) assumes that the catalytic converter is perfectly insulated and exposed to a uniform flow. The thermal gradients in the radial direction are presumed to be insignificant and both the temperature and concentration profiles are assumed to be the same in all channels. This allows the entire catalysts to be modeled with only one channel.

Siemund et al. [13] and Tischer et al. [14] measured the radial temperature profiles within ceramic TWC and found that above the light-off temperature the profile was nearly flat over the entire cross section. The experiments of Siemund et al. [13] showed that the low thermal conductivity of ceramic monoliths along with the monolith insulation guarantees that heat losses to the surroundings are negligible so that the converter is almost adiabatic. It should be remarked that the experimental data used in the present study [7] for model validation have been obtained under experimental conditions similar to those used by Siemund et al. [13].

Studies that used two dimensional (2D) (axi-symmetric) and 3D multi channel reactor models have also been reported in the literature (*e.g.*, [14,15]). From comparisons between 1D (SCM) and 2D simulations of a TWC, Tischer et al. [14] concluded that each model presents advantages and disadvantages. However, they argued that in the case of real-time simulations 1D (SCM) models are preferred. According to these authors, 2D models are necessary if the exhaust gas at the converter inlet exhibit a flow with a severe non-uniformity.

At the channel level, the most comprehensive models are based on solving the complete Navier–Stokes equations, considering both axial and radial mass, momentum and energy transport [16]. However, it is well known that the solution of the partial differential equations deriving from detailed multidimensional models is computationally expensive. In addition, 1D PFM are simpler since no diffusive terms remain in the axial direction – diffusion is assumed to be small as compared to the convective transport.

Raja et al. [16] and Groppi et al. [17] compared the performance of the 1D PFM with that of multidimensional distributed models, with both studies providing evidence of the adequacy of the 1D PFM approach. Additionally, a number of authors demonstrated the effectiveness of the 1D PFM in designing catalyst systems (*e.g.*, [13]). However, it should be stressed that the 1D PFM must be used with caution. For example, Groppi et al. [17] showed that the choice of proper correlations to evaluate the transport coefficients is critical for the adequacy of the 1D PFM, while Raja et al. [16] showed that the validity range of the 1D PFM is limited to low Reynolds numbers. Nevertheless, Raja et al. [16] suggested that the use of adequate transport coefficients may extend the applicability of the 1D PFM to high Reynolds numbers. Based on the above considerations, the 1D PFM was used in the present study.

The present 1D PFM is based on the classical simplifying assumptions, namely: the gas phase is ideal at uniform and constant pressure; constant pressure is assumed along the channel, as pressure changes are small they have negligible effect on the conversion of the reactants [13]; axial diffusion of heat and mass fluxes in the gas phase are small compared to convection and thus not considered; radiation heat transfer in the gas phase is negligible compared to convection heat transfer and hence is neglected [18]; homogeneous gas phase reactions are not considered because of the limited temperatures and small residence times of the gas stream within the monolith for typical operating conditions in automotive applications [13]; convective flux in the washcoat is irrelevant and thus neglected [6]; axial gas species diffusion in the washcoat is neglected; and there are no radial temperature gradients in the washcoat or substrate owing to the physical and geometrical properties of the washcoat/substrate and the low concentrations of reactants present.

2.2. Governing equations

With the assumptions considered in the previous section, and using the quasi steady approximation, the mass and energy balances for the gas phase become:

$$u_z \frac{\partial C_{g,j}}{\partial z} = k_{m,j} S (C_{s,j} - C_{g,j}) \tag{1}$$

$$\rho_g u_z c_{pg} \frac{\partial T_g}{\partial z} = hS(T_s - T_g) \tag{2}$$

The transport coefficients for convective mass and heat transfer in Eqs. (1) and (2) are calculated based on the Sherwood and Nusselt numbers, respectively (see Appendix A for details).

The 1D PFM approximates the washcoat with a gas–solid interface, being the mass balance for the solid phase expressed as follows:

$$\frac{\rho_g}{M_g} k_{m,j} S (C_{g,j} - C_{s,j}) = R_j \tag{3}$$

where R_j is given by:

$$R_j = \delta_C S \left(\sum_{k=1}^{N} a_{j,k} \eta_{L,k} r_k \right) \tag{4}$$

As mentioned earlier, the 1D PFM has been here modified to include the effectiveness factor, aiming at the investigation of the internal mass transfer within the washcoat. In Eq. (4) r_k accounts for the chemical kinetics and $\eta_{L,k}$ accounts for the internal mass transport within the washcoat. The method used for the evaluation of $\eta_{L,k}$, for each reaction, is presented in Appendix A and the reaction rates, r_k, are included in Appendix B.

The energy balance for the solid phase can be written as follows:

$$(1-\varepsilon)\rho_s c_{ps} \frac{\partial T_s}{\partial t} + (1-\varepsilon) k_s \frac{\partial^2 T_s}{\partial z^2} = hS(T_g - T_s) + \sum_{j=1}^{4} (-\Delta H_j) R_j \tag{5}$$

Finally, the boundary conditions for the gas phase are:

$$u_z(z=0,t) = u_{z,in}(t) \tag{6a}$$

$$T_g(z=0,t) = T_{g,in}(t) \tag{6b}$$

$$C_{g,j}(z=0,t) = C_{g,j,in}(t) \tag{6c}$$

and the boundary conditions for the solid phase are:

$$T_s(z,0) = T_{g,in}(t=0) \tag{7a}$$

$$\frac{dT_s}{dz}(0,t) = \frac{dT_s}{dz}(L,t) = 0 \tag{7b}$$

2.3. Numerical solution

In this study the finite difference method was adopted with defined space grid and time marching interval. In the numerical solution, the first step involves the computation of the temperature of the gas phase along the channel. Eq. (2) is solved by the number of transfer units (NTU) method. The gas phase domain of the channel was partitioned into discrete elements with grid space distance Δz. Subsequently, at the time step n, the gas temperature for each node $i+1$ was computed using the conditions known for the node i at time step n.

Based on the quasi steady assumption, one can compute the concentrations at the gas–solid interface and the resulting reaction rates by equating the diffusion and the reaction rates for each species j under consideration:

$$\dot{n}^n_{j,i}(C^n_{g,j,i}; C^n_{s,j,i}) = R^n_{j,i}(C^n_{s,j,i}; T^n_{s,i}) \tag{8}$$

According to Eq. (8), the rates of reaction and mass transfer to the catalytic surface are always in equilibrium, implying that there is no species accumulation on the solid catalytic surface. Expanding the first term of Eq. (8) a system of non-linear equations of the form

$$\frac{\dot{m}_g^n}{\Delta V M_g}(1 - e^{-NTUm_{j,i}^n})(C_{g,j,i}^n - C_{s,j,i}^n) = R_{j,i}^n(C_{s,j,i}^n; T_{s,i}^n) \quad (9)$$

is obtained. With the solid temperatures, $T_{s,i}$, and the gas phase concentrations, $C_{g,i,j}$, known, Eq. (9) represents a system of non-linear equations that can be solved by the method of Newton at each node i to obtain the solid phase concentrations. Subsequently, the gas phase concentrations can be computed using the NTU method.

Together with the boundary conditions expressed by Eqs. (7a) and (7b), Eq. (5) can be solved for the solid temperature, T_s, using the forward-time and centered-space finite difference discretisation.

Finally, the stability criterion for this numerical method is:

$$\alpha_s \frac{\Delta t}{\Delta z^2} \leq \frac{1}{2} \quad (10)$$

Based on the space length of the channel, the space grid (Δz) chosen was 2 mm and the corresponding time step-size (Δt) 1 s. With these values the model stability criteria was satisfied for all tests.

3. Model validation

Table 1 shows the model input parameters for the gas and the ceramic substrate properties. The gas specific heat capacity, the dynamic viscosity and the thermal conductivity were calculated from appropriate formulas provided by Brinkmeier [19]. The correlations presented in Table 1 for the gas diffusivities were determined based on the procedure described in McCullough et al. [20] and the correlations included in the table for the effective diffusivities were based on experimental data recently available in the literature [21,22]. The solid (ceramic substrate) properties were based on literature data from the manufactures [23,24].

Table 2 shows the model input parameters for the numerical simulation of 3 of the 18 steady-state tests studied experimentally by Santos and Costa [7]. The table includes the measurements at the TWC inlet for these three operating conditions, which represent operation at the lowest inlet temperature and mass flow rate (operating condition 1), at the highest inlet temperature and mass flow rate (operating condition 18), and at an intermediate condition (operating condition 9) of those conditions studied by Santos and Costa [7].

Table 1
Model input parameters for gas and ceramic substrate properties.

(a) Gas properties	
Density ($kg\,m^{-3}$)	Ideal gas law, $\rho_g = P_g/R_p T_g$
Specific heat capacity ($J\,kg^{-1}\,K^{-1}$)	$c_{pg} = 981.76 + 0.2357T_g + 1.0 \times 10^{-4}T_g^2 - 6.0 \times 10^{-8}T_g^3$
Dynamic viscosity ($N\,s\,m^{-2}$)	$\mu_g = 10^{-6} \times (4.666 + 0.04796T_g - 0.000011T_g^2)$
Thermal conductivity ($W\,m^{-1}\,K^{-1}$)	$k_g = 10^{-3} \times (7.151 + 0.06557T_g - 6.871 \times 10^{-6}T_g^2)$
Gas diffusivities ($m^2\,s^{-1}$)	$D_{g,CO} = 9.6502 \times 10^{-5}(T_g^{1.75}/P_g)$
	$D_{g,H_2} = 34.805 \times 10^{-5}(T_g^{1.75}/P_g)$
	$D_{g,C_3H_7} = 5.6240 \times 10^{-5}(T_g^{1.75}/P_g)$
	$D_{g,NO} = 11.2065 \times 10^{-5}(T_g^{1.75}/P_g)$
	$D_{g,O_2} = 9.6500 \times 10^{-5}(T_g^{1.75}/P_g)$
Effective diffusivities ($m^2\,s^{-1}$)	$D_{eff,CO} = 13.31 \times 10^{-4}(T_s^{0.5}/P_g)$
	$D_{eff,H_2} = 49.812 \times 10^{-4}(T_s^{0.5}/P_g)$
	$D_{eff,C_3H_7} = 8.834 \times 10^{-4}(T_s^{0.5}/P_g)$
	$D_{eff,NO} = 12.858 \times 10^{-4}(T_s^{0.5}/P_g)$
	$D_{eff,O_2} = 12.45 \times 10^{-4}(T_s^{0.5}/P_g)$
(b) Ceramic substrate properties	
Specific heat capacity ($J\,kg^{-1}\,K^{-1}$)	$c_{ps} = -3.435 \times 10^7/T_s^2 + 1071.0 + 0.156T_s$
Density of substrate ($kg\,m^{-3}$)	$\rho_s = 1770$
Thermal conductivity ($W\,m^{-1}\,K^{-1}$)	$k_s = 1$

Table 2
Model input parameters for the simulation of typical steady-state tests.

	Operating condition		
	1	9	18
(a) Exhaust gas composition at TWC inlet, percentage (%)			
Gas			
CO	0.616	0.913	0.790
H_2	0.205	0.304	0.260
C_3H_7	0.0231	0.0324	0.0147
NO	0.0241	0.1547	0.3134
O_2	0.4984	0.6706	0.4381
(b) Flow parameters			
Mass flow rate ($kg\,s^{-1}$)	0.0121	0.0353	0.0740
Inlet gas temperature (K)	595	822	1018
(c) Initial conditions			
Initial solid temperature = inlet gas temperature			
(d) Ambient conditions			
Atmospheric temperature (K)		298.15	
Atmospheric pressure (Pa)		101325	

Appendix B presents in detail the reaction scheme along with the semi-empirical rate expressions [25] used in the present study (see Table B.1). These expressions contain parameters that must be estimated by fitting the model to a set of experimental data, which represent the behavior of the TWC under typical operating conditions. A number of authors (*e.g.*, [13,23]) showed that this approach gives satisfactory results. Table B.2 shows the reaction parameters obtained by fitting the pre-exponential factor and the activation energy of the rate expressions. It is important to note that the parameters presented in Table B.2 are specific of the TWC used in the present study. However, these parameters do not lump the internal mass transfer effects as in Siemund et al. [13] and Holder et al. [23], among others.

Fig. 1 shows the predicted and measured gas and solid temperatures along a channel of the TWC for operating condition 9. Both the solid and gas temperatures profiles displayed in Fig. 1 are typical of TWC operation above the light-off temperature. The differences observed between the solid and the gas temperatures confirm the adequacy of the 1D PFM with the effectiveness factor implemented.

Fig. 1 shows that the predicted solid temperatures are always above the predicted gas temperatures – it is well known that above the light-off temperature the entire reactor is ignited so that the heat of reaction produced within the washcoat leads to higher solid temperatures. The maximum difference between the solid and gas temperatures occur at the inlet region, with this difference decreasing along the axial direction up to the channel exit, where the

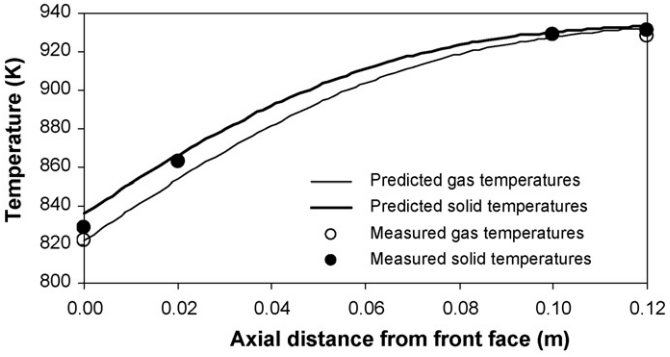

Fig. 1. Predicted and measured gas and solid temperatures along a channel of the TWC for operating condition 9.

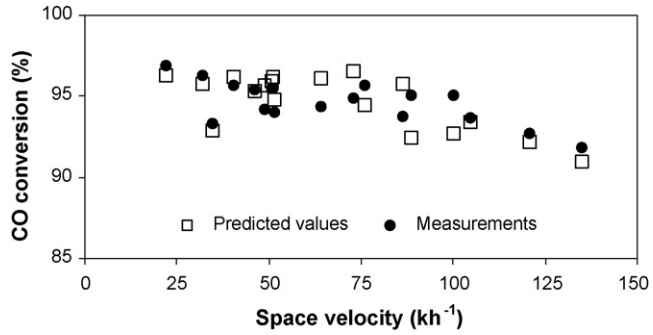

Fig. 2. Predicted and measured CO conversion as a function of space velocity for the 18 steady-state tests studied by Santos and Costa [7].

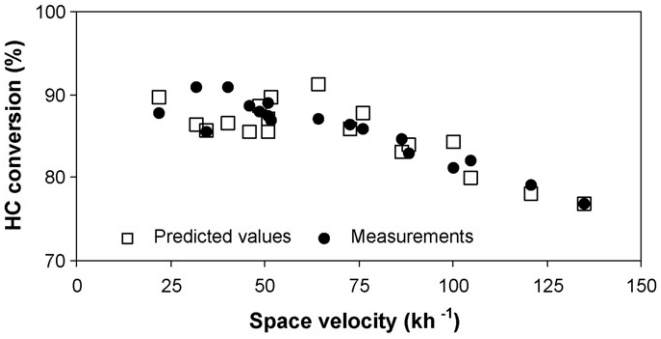

Fig. 3. Predicted and measured HC conversion as a function of space velocity for the 18 steady-state tests studied by Santos and Costa [7].

difference reaches a minimum. This is because the heat produced by the catalytic reaction is superior at the channel inlet, that is, the chemical species conversion is more extensive at the inlet region where the concentrations of the CO, HC and NO_x are higher.

Fig. 1 also reveals that the four measured solid temperature values lie in between the predicted solid and gas temperature values, as one could have anticipated. It is seen that at the rear section of the channel the predicted solid temperature values are closer to the measured ones. Note that at the reactor exit, where the gas and solid temperatures are similar, the influence of the gas temperature on the solid temperature measurement is minimum, which indicates the accuracy of the predictions.

Finally, Fig. 1 shows that the predicted gas temperatures at the TWC exit are rather close to the measured values for the three operating conditions. This has also been observed for the remaining operating conditions studied by Santos and Costa [7]. In this earlier work, we have not performed gas temperature measurements within the channel along the axial direction. The predicted gas temperature profiles reveal, however, the expected trends.

Figs. 2–4 show comparisons between the predicted and measured conversions as a function of space velocity for CO, HC and NO_x, respectively. Note that each figure presents the experimental data for the 18 steady-state tests studied by Santos and Costa [7] and it is seen that the present model predicts accurately the measured conversions.

It was verified that the 1D PFM without the effectiveness factor strongly over predicts the experimental measured conversions.

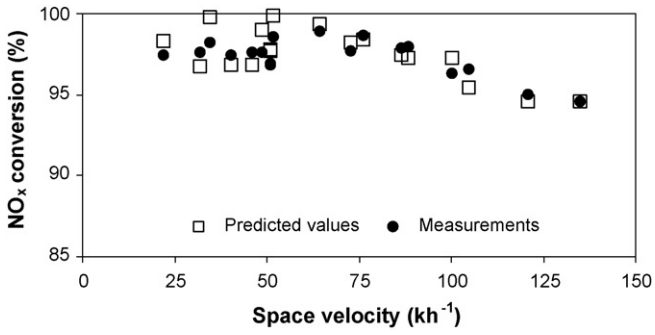

Fig. 4. Predicted and measured NO_x conversion as a function of space velocity for the 18 steady-state tests studied by Santos and Costa [7].

Table 3
Main technical attributes of the catalyst considered.

Substrate type	Square cell ceramic
Cell density (cells cm^{-2})	62 (400 cpsi)
Substrate dimensions (mm)	Diameter = 127; L = 120
Catalyst volume (dm^3)	1.52
Coated geometric surface area ($m^2\ m^{-3}$)	2526
Uncoated wall thickness (mm)	0.1651 (6.5 mil)
Mean washcoat thickness (mm)	0.025
Open frontal area coated (%)	69.0
Cell hydraulic diameter uncoated (mm)	1.105
Washcoat material	CeO_2–Al_2O_3
Precious metal loading	7 Pd/1 Rh
Total mass of precious metal (g)	1.159

A comparison between the 1D PFM with and without the effectiveness factor implemented reveals that the predictions with the latter approach are always above of those obtained with the former approach presented in Figs. 2–4. This result is consistent with the findings of Kryl et al. [26], who verified that neglecting the diffusion in the washcoat leads to a significant overestimation of the conversions.

4. Influence of the channel and washcoat structures on TWC conversions

The present section concentrates on both turbulent monolith structures and controlled washcoat structures, being its main objective to analyze numerically the importance of these design parameters on TWC conversions.

Table 3 lists the main characteristics of the TWC considered here and Table 4 summarizes the channel and washcoat structures analyzed numerically here. Section 4.1 presents and discusses the baseline condition, Section 4.2 presents and discusses the two conditions related with the channel structure and, finally, Section 4.3 presents and discusses one condition related with the washcoat structure. Both Sections 4.2 and 4.3 start with justifications for the structures selected for this study.

4.1. Baseline structure

For the baseline structure (see Table 4), Figs. 5 and 6 show the predicted conversions as a function of the space velocity for the

Table 4
Channel and washcoat structures analyzed.

Structure	Baseline	Channel structure with moderate protrusions	Channel structure with intense protrusions	Improved washcoat structure
TWC	See Table 3	See Table 3	See Table 3	See Table 3
Flow	Laminar	$Sh = 2Sh_{laminar}$	$Sh = 10Sh_{laminar}$	Laminar
Effective diffusivities	See Table 1	See Table 1	See Table 1	$D_{eff} = 2D_{eff,ref}$

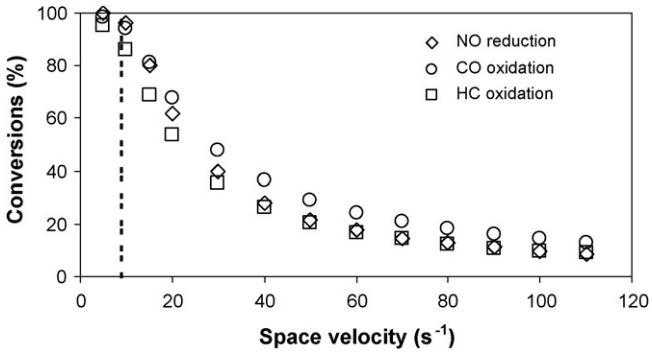

Fig. 5. Predicted conversions as a function of the space velocity for the operating condition 1.

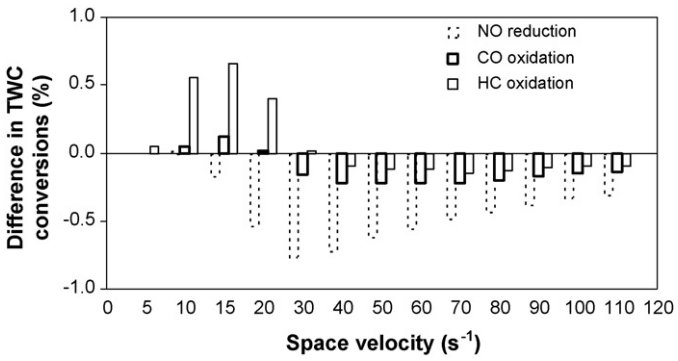

Fig. 7. Predicted differences, relative to the baseline structure, in TWC conversions as a function of the space velocity for a channel structure with moderate protrusions ($Sh = 2Sh_{laminar}$) for the operating condition 1.

operating conditions 1 and 18, respectively (see Table 2). The space velocity used in these figures is referenced to 273.15 K and the vertical dashed line in Figs. 5 and 6 represents the space velocity used in the experiments that corresponds to the inlet mass flow rate given in Table 2.

Figs. 5 and 6 reveal that the baseline structure achieves conversions close to 100% only at small space velocities. It is seen that as the space velocity increases the TWC conversions decrease markedly. In addition, the figures show that for a given space velocity the TWC reaches higher conversions as the inlet gas temperature increases.

Under most operating conditions relevant for an automotive exhaust system the TWC conversions are limited by the transport phenomena [1,27]. In this respect, the critical parameters that most affect the TWC conversions are the transport coefficients and the effective diffusivities that control the external and internal mass transfer phenomena, respectively. Accordingly, design improvements in the TWC require an accurate knowledge of the effect of both channel and washcoat structures in the TWC conversions, as discussed below.

4.2. Influence of the channel structure on TWC conversions

Mass and heat transfer effects in TWC monoliths have been widely investigated in the laminar flow region for a variety of channels shapes and operating conditions. At the entrance of a channel the concentration profiles are flat and the local reaction rates high. Further downstream of the channel the flow develops to laminar and the mass transfer limits the reaction. The external mass and heat transfer decreases logarithmically from a high value at the entrance to an asymptotic value in the fully developed region.

Decreasing the channel diameter by increasing the substrate cell density enhances the mass transfer coefficient. In addition, the mass transfer coefficient increases at higher gas velocities, that is, higher Reynolds numbers. However, laminar flow conditions are unfavorable for mass and heat transfer as compared to turbulent flow conditions.

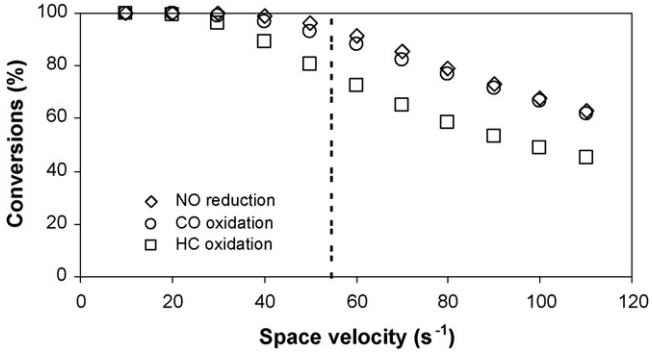

Fig. 6. Predicted conversions as a function of the space velocity for the operating condition 18.

Holmgren [9] and Haas and Rice [10] found that the protrusions in the channel walls increase the mass transfer rate, expressed as the Sherwood number, being the increase higher when the Reynolds number was increased. The roles of the protrusions in the channel walls used in the turbulent monolith structures are: (i) to disturb the boundary layers, (ii) to generate swirl and vortices, and (iii) to destabilize the flow or to intensify the turbulence.

These channel structures increase the local mass transfer coefficient. Note, however, that a fully turbulent catalytic converter would have a very high pressure drop. For this reason, the so-called turbulent monolith structures generate the turbulence locally, which minimizes the adverse effect of the pressure drop increase.

It has been established that the use of protrusions in channel walls may significantly reduce the critical Reynolds number at which transition to turbulent flow takes place; in fact, critical Reynolds numbers below 700 have been reported [28]. Even for Reynolds numbers of about 250–300, Holmgren [9] found that obstacles produce non-steady disturbances in the flow.

There are many complexities in the computation of accurate heat and mass transfer coefficients in monolith reactors, especially in the transition flow. However, based on the literature (*e.g.*, [9,10]), it is secure to assume that the range of Nusselt and Sherwood numbers over the expected operation interval of TWC using the so-called turbulent monolith structures will be 1–10 times higher than that corresponding to laminar flow conditions.

To demonstrate the effect of the turbulent monolith structures on TWC conversions, we have here compared the baseline structure (laminar monolith) with turbulent monolith structures with the same dimensions and properties but with Nusselt and Sherwood numbers 2 and 10 times higher than those of the laminar flow conditions.

Figs. 7 and 8 show the predicted differences, relative to the baseline structure, in TWC conversions as a function of the space velocity for a channel structure with moderate protrusions ($Sh = 2Sh_{laminar}$) for the operating conditions 1 and 18, respectively, and Figs. 9 and 10 show the predicted differences, relative to the baseline structure, in TWC conversions as a function of the space velocity for a channel structure with intense protrusions ($Sh = 10Sh_{laminar}$) for the operating conditions 1 and 18, respectively.

Figs. 7–10 reveal that the most positive effect of the transport coefficients on the TWC conversions is observed for the HC followed by the CO and NO_x, respectively, regardless of the inlet gas temperature, *i.e.*, of the operating condition. As can be seen, the increase in the TWC conversions are higher for $Sh = 10Sh_{laminar}$. However,

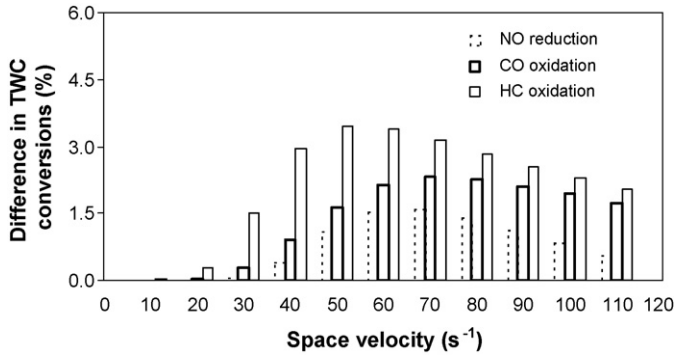

Fig. 8. Predicted differences, relative to the baseline structure, in TWC conversions as a function of the space velocity for a channel structure with moderate protrusions ($Sh = 2Sh_{laminar}$) for the operating condition 18.

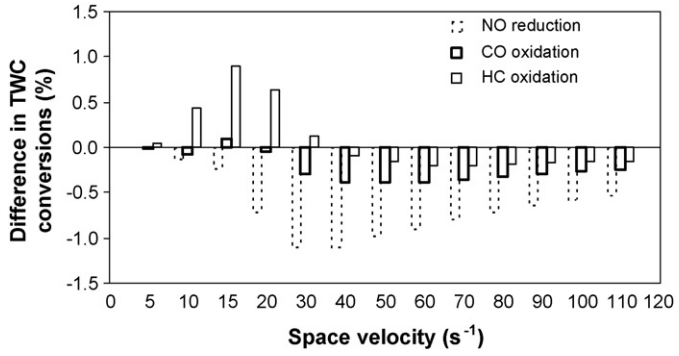

Fig. 9. Predicted differences, relative to the baseline structure, in TWC conversions as a function of the space velocity for a channel structure with intense protrusions ($Sh = 10Sh_{laminar}$) for the operating condition 1.

since the differences between the numerical data obtained for $Sh = 2Sh_{laminar}$ and $Sh = 10Sh_{laminar}$ are relatively small a monolith structure with $Sh = 2Sh_{laminar}$ is adequate to achieve higher conversions with a minor back-pressure penalty [9].

It is noticeable in Figs. 7–10 that at low inlet gas temperatures the TWC conversions are less dependent of the transport coefficients. In addition, the present numerical results demonstrate that increasing the transport coefficients using turbulent monolith structures can produce either positive or negative effects on the TWC conversions, as shown in Figs. 7 and 9. However, Figs. 8 and 10 demonstrate that for higher inlet gas temperatures the turbulent monolith structures present important improvements in the TWC conversions.

The main objective of using turbulent monolith structures is to improve the external transport phenomena between the bulk gas phase and the washcoat surface. It should be noted, however, that there are two circumstances where increased heat and mass transfer coefficients can decrease the reaction rate and hence the TWC conversions: a decrease in wall temperature that decelerates the reaction rate more than an increase in wall concentration accelerates it, and an increase in the wall concentration of reactants that inhibits the reaction. At operating conditions above the light-off temperature the latter effect has a marginal impact in the reaction rates and thus can be ignored in the present study. In regard to the former effect, however, it is important to note that the increase in the transport coefficients increase simultaneously mass and heat transport. At temperatures below light-off the increase in the heat transport coefficients contributes positively to heat up the solid (washcoat and substrate) reducing thereby the heating period of the TWC.

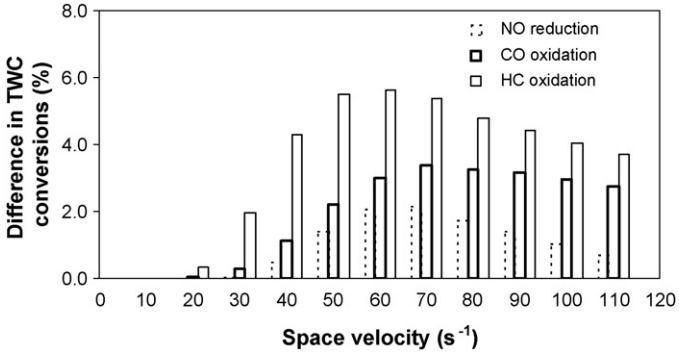

Fig. 10. Predicted differences, relative to the baseline structure, in TWC conversions as a function of the space velocity for a channel structure with intense protrusions ($Sh = 10Sh_{laminar}$) for the operating condition 18.

Nevertheless, above light-off temperature the wall temperature is always higher than the gas temperature and hence the heat flux occurs from the wall to the gas. Thus, increasing the transport coefficients contributes to increase the wall concentration of reactants and to remove the wall products back to the bulk-gas phase. But, because heat transfer is also enhanced, the heat transfer to the gas flow increases and therefore the wall temperature decreases. In part, due to this effect the reactions proceed at slower rates. Thus, at operating temperatures above light-off the increase in the transport coefficients is beneficial to the mass transfer but is detrimental to the heat transfer.

Figs. 8 and 10 reveal that for an inlet gas temperature of 1018 K the TWC conversions increase with increasing transport coefficients, regardless of the space velocity. These results indicate that at higher inlet gas temperatures the external mass transport of reactants and products is very important to improve the TWC conversions. Here, the decrease in the wall temperature is clearly compensated by the improvements achieved in the mass transport.

In summary, the net effect of increasing the transport coefficients on the TWC conversions is positive. In addition, higher transport coefficients have the advantage of reducing the local hot-spots and the maximum operating temperature which prevents the thermal deactivation and hence increases the TWC life time. These features allow the use of turbulent monolith structures closer to the engine as compared with classical laminar monolith structures used today in pre-catalysts and cascade systems.

4.3. Influence of the washcoat structure on TWC conversions

Internal diffusion of the gas species into the porous solid structures that include macro pore, meso pore and micro pore diffusion depends on the pore diameter. Recently, a number of studies [21,22,29,30] have used several techniques for obtaining pore transport characteristics in commercial available washcoat layers. Typical sizes of pore diameter in a TWC washcoat range from 6.5 nm to 500 nm [29], so that micro pore diffusion may be neglected.

The washcoat structure can be characterized by the pore diameters d_p, porosity ε_p, and the tortuosity factor, τ. Tortuosity, porosity and mean pore diameter were measured experimentally for TWC washcoats by Hayes et al. [29].

There are two main theoretical models to define the effective diffusivity as a function of the washcoat structure: the random pore model and the parallel pore model. Hayes et al. [29] have concluded that the random pore model is not appropriate for monolith washcoats and recommended the use of the parallel pore model for an alumina washcoat. The results predicted by the parallel pore model agree well with the experimental results [21,22,29,30], and thus when data is unavailable but the fundamental parameters of the washcoat structure are known, this model is appropriate to predict the effective diffusivity of the TWC washcoat.

The typical CeO_2–Al_2O_3 washcoat, widely used today in commercial TWC, has a bi-modal pore size distribution composed mainly by small meso pores of about 10 nm and by macro pores (pore diameter in the range of 100–500 nm and volume fraction around 20%) [4,22].

Suárez et al. [11] produced porous materials with a remarkable increase in the macro pore volume as compared with commercial materials of the same composition and demonstrated that this leads to an increase in the effectiveness factor. Yuan and Su [12] demonstrated that the incorporation of hierarchical materials containing both interconnected bi-modal meso and macro porous structures and defined morphologies have enhanced proprieties as compared with single size meso porous materials. The meso and macro porous washcoat structure combines the benefits of reduced resistance to diffusion and high surface areas for adsorption and reaction.

According to the parallel pore model, the porous washcoat structure can be taken into account by application of the effective diffusivity that leads to:

$$D_{eff,j} = \frac{\varepsilon_p D_j}{\tau} \tag{11}$$

where D_j is a diffusivity that combines the effects of the bulk diffusion, $D_{b,j}$ (macro pore), and of the Knudsen diffusion, $D_{K,j}$ (meso pore), defined as follows:

$$D_j = \frac{V_{meso}/V_{total}}{(1/D_{b,j}) + (1/D_{K,j})} + \frac{V_{macro}/V_{total}}{(1/D_{b,j}) + (1/D_{K,j})} \tag{12}$$

The volume diffusion was calculated as it was done for the gas phase (see Table 1). The Knudsen diffusion can be calculated as:

$$D_{K,j} = 48.5 d_p \sqrt{\frac{T_s}{10^3 M_j}} \tag{13}$$

Based on recent results [11,12], we have concluded that enhanced washcoat structures allowed for a substantial increase in macro pores volume.

In order to demonstrate the influence of the improved washcoat structures on the effective diffusivities, a CeO_2–Al_2O_3 washcoat structure composed by 80% of meso pores and 20% of macro pores with pore diameters of 10 and 130 nm, respectively, was considered as the baseline.

Two improved washcoat structures have been considered here: 80% 10 nm + 20% 400 nm and 60% 10 nm + 40% 130 nm. The effective diffusivities for these washcoat structures have been evaluated using Eqs. (11)–(13). Note that the tortuosity factor and the porosity of the washcoat depend on the washcoat structure. The study of Hayes et al. [29] indicates that the tortuosity factor and the porosity of a commercial TWC washcoat are 8.1 and 0.41, respectively. Due to the lack of experimental data it was assumed that these parameters remain unchanged for the two improved washcoat structures considered here.

Fig. 11 shows predicted effective diffusivities as a function of the temperature for the three different washcoat structures. It can be observed that the dependence of the effective diffusivity on the temperature changes both with the percentage of macro pores and with the diameter of macro pores. This occurs because the volume diffusion increases more with the temperature than the Knudsen diffusion; specifically, the temperature dependence is $T^{1.75}$ for the volume diffusion and $T^{0.5}$ for the Knudsen diffusion.

Fig. 11 demonstrates that for the temperature range studied here the effective diffusivity may increase by a factor of about 2 as compared to the baseline washcoat. In order to study the effect of improving the internal mass transfer with enhanced washcoat structures, the effective diffusivity of the baseline washcoat (see Table 1) has been multiplied by 2, with all remaining washcoat properties being kept constant (see Table 4).

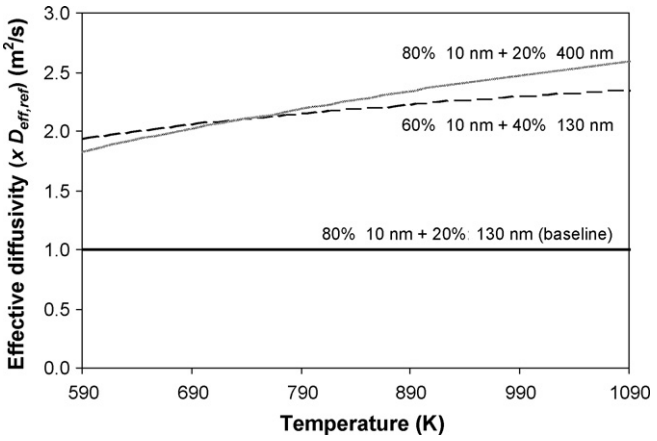

Fig. 11. Predicted effective diffusivities as a function of temperature for three different washcoat structures.

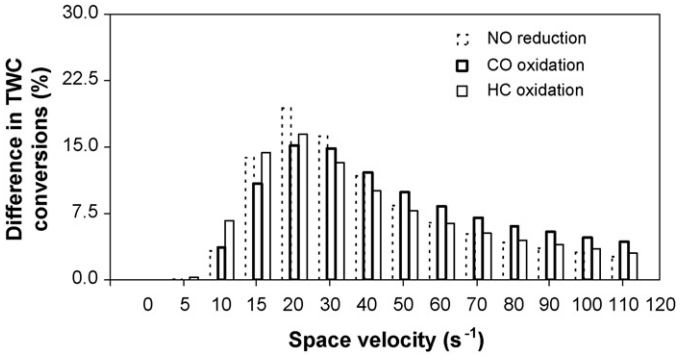

Fig. 12. Predicted differences, relative to the baseline structure, in TWC conversions as a function of the space velocity for an improved washcoat structure ($D_{eff} = 2D_{eff,ref}$) for the operating condition 1.

Figs. 12 and 13 show the predicted differences, relative to the baseline structure, in TWC conversions as a function of the space velocity for an improved washcoat structure ($D_{eff} = 2D_{eff,ref}$) for the operating conditions 1 and 18, respectively.

The results in Figs. 12 and 13 demonstrate that the baseline TWC structure suffered from internal mass transfer limitations. It is seen that the TWC reaches higher conversions as the effective diffusivities attain higher values regardless of the chemical species. Note that as the effective diffusivity increases the transverse diffusion time for the mass transport of reactants and products within the washcoat decreases. Thus, the internal mass transfer process is enhanced and a more uniform concentration gradient throughout

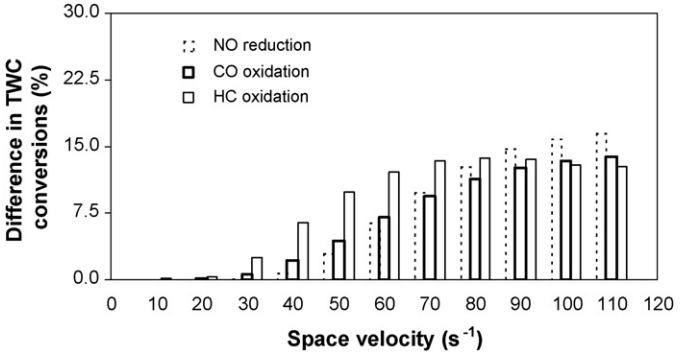

Fig. 13. Predicted differences, relative to the baseline structure, in TWC conversions as a function of the space velocity for an improved washcoat structure ($D_{eff} = 2D_{eff,ref}$) for the operating condition 18.

the washcoat is achieved. This leads to a better washcoat utilization and thus to higher TWC conversions. In addition, the increase of the reactants availability in the catalytic active sites leads to an increase in the reaction rates which permit to attain higher wall operating temperatures. As a consequence, the reaction time within the catalytic layer decreases contributing to increase the reactants conversion.

Figs. 12 and 13 also demonstrate that the improvements in the TWC conversions using washcoat structures that provide higher effective diffusivities depend on the space velocity. It is interesting to note that for the inlet gas temperature of 595 K (see Fig. 12) the improvements in the TWC conversions attain the maximum effect at intermediate space velocities. However, as the inlet gas temperature increases the maximum effect of the effective diffusivities in the TWC conversions occurs for higher space velocities. In addition, the TWC conversions depend also on the reaction time of the catalytic layer which decreases as the inlet gas temperature increases. Because of this, at low inlet gas temperatures (*e.g.*, 595 K), the influence of the external mass transport in the TWC conversions is noticeable at lower space velocities owing to the higher reaction time of the catalytic layer as compared to the reaction time at higher inlet gas temperatures.

In light of the results presented above, it can be concluded that increasing effective diffusivities has a more significant impact on TWC conversions than increasing the transport coefficients. Therefore, improvements in the transport properties of the washcoat structure is the most critical design challenge to augment TWC conversions above the light-off temperature.

The design options also depend on thermal and mechanical constrains. In this context, the increase in the transport coefficients contributes to decrease the maximum wall operating temperature of the TWC. In contrast, the increase in the effective diffusivities contributes to increase the maximum wall operating temperature of the TWC. Because of this, the formation of hot-spots and thus the thermal deactivation is critical when the percentage of macro pores in the washcoat structure increases. In addition, the increase in the macro pore volume generally reduces the mechanical resistance of the porous structure [11]. For this reason, the use of macro pore washcoat structures in TWC installed closer to the engine needs to be careful analyzed.

5. Conclusions

A single channel model accounting for the species diffusion inside the washcoat using the effectiveness factor was developed. Validation and calibration of the model was achieved by comparing predictions against experimental data. Predictions of gas and solid temperature profiles as well as of TWC conversions demonstrate the adequacy of the 1D PFM with the effectiveness factor implemented. The model was then applied to study the importance of both turbulent monolith structures and controlled washcoat structures on TWC conversions being the main conclusions as follows:

(i) increasing the transport coefficients using turbulent monolith structures can produce either positive or negative effects on the TWC conversions;
(ii) overall, the net effect of increasing the transport coefficients on the TWC conversions is positive;
(iii) at high inlet gas temperatures and high space velocities the turbulent monolith structures present important improvements in the TWC conversions;
(iv) the TWC conversions can be significantly improved enhancing the transport properties of the porous washcoat structure;
(v) enhancements in the transport properties of the washcoat structure have deeper impacts on the TWC conversions than improvements in the monolith channel structure.

Acknowledgement

The first author (H. Santos) is pleased to acknowledge the Fundação para a Ciência e Tecnologia for the provision of a scholarship SFRH/BD/32851/2006.

Appendix A. Transport phenomena

External mass transfer – transport coefficients

The external transport phenomena between the gas and the gas–solid interface in the 1D PFM is accounted for through the heat and mass transfer transport coefficients. It is well known that the development of thermal and concentration boundary layers is completed near the entrance of the TWC channels and a fully developed laminar boundary layer is thus formed in most part of the reactor. In order to take into account the enhanced transfer rates found in the entrance region, the 1D PFM used in this study uses a simultaneously developing velocity, concentration and thermal boundary layer, with heat and mass transfer coefficients dependent of the position and velocity, without solving the Navier–Stokes equations. As shown by Balakotaiah and West [31], the solution of momentum balance can be avoided in laminar boundary layers by using heat and mass transfer correlations.

For the case of developing velocity, concentration and thermal boundary layers, Ramanathan et al. [32] presented the following expressions to give the Sherwood and Nusselt numbers along the channel:

$$Sh_j(z) = \begin{cases} \dfrac{1.4}{Sc_j^{1/6}}\left(\dfrac{R_\Omega^2 u_z}{zD_{g,j}}\right)^{1/2}, & 0 < z < \dfrac{R_\Omega^2 u_z}{D_{g,j}}\dfrac{1}{Sc_j^{1/3}}\left(\dfrac{1.4}{Sh_{T,\infty}}\right)^2 \\ Sh_{T,\infty}, & z \geq \dfrac{R_\Omega^2 u_z}{D_{g,j}}\dfrac{1}{Sc_j^{1/3}}\left(\dfrac{1.4}{Sh_{T,\infty}}\right)^2 \end{cases} \tag{A.1}$$

$$Nu(z) = \begin{cases} \dfrac{1.4}{Pr^{1/6}}\left(\dfrac{R_\Omega^2 u_z}{z\alpha_g}\right)^{1/2}, & 0 < z < \dfrac{R_\Omega^2 u_z}{\alpha_g}\dfrac{1}{Pr^{1/3}}\left(\dfrac{1.4}{Nu_{T,\infty}}\right)^2 \\ Nu_{T,\infty}, & z \geq \dfrac{R_\Omega^2 u_z}{\alpha_g}\dfrac{1}{Pr^{1/3}}\left(\dfrac{1.4}{Nu_{T,\infty}}\right)^2 \end{cases} \tag{A.2}$$

Internal mass transfer – effectiveness factor

As of today, the approach of neglecting the internal mass transfer has been usually preferred in the TWC numerical modelling for its simplicity. Modelling studies on mass transport within the porous washcoat (*e.g.*, [5,6,33–35]) demonstrate that under certain circumstances the internal mass transfer can be successfully incorporated using the effectiveness factor model, so that the model is maintained simple and its needs in terms of computational time low. When the effectiveness factor model is used, the reaction rate constant, $k_{V,k}$, is evaluated using the following equation:

$$k_{V,k} = \frac{r_k}{C_{ref}} \tag{A.3}$$

For kinetic laws, others than first-order, the generalized Thiele modulus may be used [35]. After evaluated $k_{V,k}$, using Eq. (A.3), the generalized Thiele modulus can be defined as:

$$\phi_{L,k} = \delta_c \sqrt{\frac{k_{V,k}}{D_{eff,k}}} \tag{A.4}$$

This method assumes a homogeneous porous medium that considerers $D_{eff,k}$ constant and uses a geometric characteristic length,

δ_c, for any geometry as the ratio of the catalyst volume to the external surface area. The thickness of the catalytic layer of the present ceramic TWC is very small (25 μm) so that the washcoat may be viewed as an infinite slab (flat-plate) with a geometric characteristic length δ_c (see Fig. 1). Given that, the generic solution for the effectiveness factor can be approximated by [36]:

$$\eta_{L,k} = \frac{\tanh(\phi_{L,k})}{\phi_{L,k}} \quad (A.5)$$

The above analysis is exact for a chemical species that dissociates isothermally in the catalytic washcoat, following a first order reaction rate. Zygourakis and Aris [5] observed the validity of the isothermal washcoat assumption using the Prater relation. They concluded that for reactant concentrations encountered in automotive TWC, the temperature change within the washcoat is less than 1 K.

In the case of other kinetic laws (*e.g.*, LHHW), Eq. (A.5) may also give a good approximation if the generalized Thiele modulus Eq. (A.4) is used [35]. Examples of LHHW behavior can be found in Leung et al. [33], Papadias et al. [35] and Hayes et al. [37,38], among others.

At the highest temperatures, where most of the reaction takes place near the exposed surface of the washcoat, the effectiveness factors converge to the exact asymptotic expression, $\eta_{L,k} = 1/\phi_{L,k}$, and therefore there is no differences between 1D effectiveness factor model and 2D detailed models. Papadias et al. [35] used LHHW kinetics for the CO oxidation reaction to show that in the asymptotic region, with temperatures above 500 K, the agreement between 1D and 2D methods for calculating effectiveness factors is very good.

Zygourakis and Aris [5] and Wanker et al. [6] also showed that the 1D effectiveness factor model is adequate for temperatures above light-off and low reactants concentrations, typical of exhaust aftertreatment systems such as TWC. Note that, for the operating conditions studied in the present work, the temperature is always above 595 K, and the reactants concentration of CO at the TWC inlet are in between 0.58% and 0.97% (the inlet concentrations of HC and NO_x are lower than those of the CO). Thus for the present modelling study, one can conclude that the effectiveness factor model is adequate even with LHHW kinetics.

Appendix B. Chemical reactions

The reaction scheme used in the present study is based on four dominant reactions that correspond to the oxidation of CO, H_2 and HC and to the NO reduction by CO. H_2 oxidation is taken into account due to the substantial heat production associated with it; its reaction kinetics may be handled with no difficulty since they are closely related to CO oxidation kinetics [39]. Regarding the HC oxidation, the usual approach is to assume two species, the fast and the slow oxidizing ones [39]: 86% of fast oxidizing hydrocarbons (C_3H_6) and 14% of slow oxidizing hydrocarbons (CH_4). In order to avoid any superfluous complexity, it was decided to model here the HC only as C_3H_7. This approach reproduces accurately the HC oxidation, as verified by Konstantas [40]. The reduction of NO is due to its reactions with reducing agents such as CO, H_2 and HC. In the TWC, CO is considered to be the main species participating in NO reduction [13,39,40].

It is assumed that the reactions above are dominant. Several other catalytic reactions occur inside the TWC washcoat, depending on the exhaust gas composition, temperature and washcoat composition of the catalyst [41]. But they seem to have negligible effects or are too slow to compete with the dominant reactions [25]. Single step global rate equations favor the simplification of the reaction scheme. Note that above the light-off temperature the TWC conversion is dominated by transport phenomena, thus the global kinetic rates should fulfill the requirement of the study, being the surface adsorption–desorption and the intrinsic reaction included in the global kinetic rate expressions. A common practice in the literature is also to lump the internal mass transfer in these global kinetic rate expressions.

The chemical reactions take place in many complicated steps [42]. However, most of the existing models rely on LHHW type

Table B.1
Reaction scheme and rate expressions used in the present study.

	Reaction	Rate expression
Oxidation reactions		
1	$CO + 0.5\,O_2 \rightarrow CO_2$	$r_1 = \frac{A_1 e^{(-E_{a1}/R_g T_s)} C_{CO} C_{O_2}}{G}$
2	$H_2 + 0.5\,O_2 \rightarrow H_2O$	$r_2 = \frac{A_2 e^{(-E_{a2}/R_g T_s)} C_{H_2} C_{O_2}}{G}$
3	$C_3H_7 + 4.75\,O_2 \rightarrow 3\,CO_2 + 3.5\,H_2O$	$r_3 = \frac{A_3 e^{(-E_{a3}/R_g T_s)} C_{C_3H_7} C_{O_2}}{G}$
Inhibition term	$G = T_s(1 + K_1 C_{CO} + K_2 C_{C_3H_7})^2 (1 + K_3 C_{CO}^2 C_{C_3H_7}^2)(1 + K_4 C_{NO}^{0.7})$; $K_i = k_i e\left(-\frac{\Delta Ha_i}{R_g T_s}\right)$ $k_1 = 65.5$, $k_2 = 2080$, $k_3 = 3.98$, $k_4 = 479000$ $\Delta Ha_1 = -7990$, $\Delta Ha_2 = -3000$, $\Delta Ha_3 = -96534$, $\Delta Ha_4 = 31036$	
Reduction reaction		
4	$CO + NO \rightarrow CO_2 + 0.5N_2$	$r_4 = \frac{A_4 e^{(-E_{a4}/R_g T_s)} C_{CO} C_{NO}}{G}$
Inhibition term	$G = T_s(1 + K_1 C_{CO} + K_2 C_{C_3H_7})^2 (1 + K_3 C_{CO}^2 C_{C_3H_7}^2)(1 + K_4 C_{NO}^{0.7})$; $K_i = k_i e\left(-\frac{\Delta Ha_i}{R_g T_s}\right)$ $k_1 = 400$, $k_2 = 200$, $k_3 = 3.98$, $k_4 = 200000$ $\Delta Ha_1 = -7990$, $\Delta Ha_2 = -3000$, $\Delta Ha_3 = -96534$, $\Delta Ha_4 = 31036$	

Table B.2
Reaction parameters.

	Reaction	Pre-exponential factor (mol K m^{-3} s^{-1})	Activation energy (J mol^{-1})
1	$CO + 0.5\,O_2 \rightarrow CO_2$	$A_1 = 1.34 \times 10^{18}$	$E_{a1} = 84000$
2	$H_2 + 0.5\,O_2 \rightarrow H_2O$	$A_2 = 1.34 \times 10^{18}$	$E_{a2} = 84000$
3	$C_3H_7 + 4.75\,O_2 \rightarrow 3\,CO_2 + 3.5\,H_2O$	$A_3 = 6.9 \times 10^{18}$	$E_{a3} = 94000$
4	$CO + NO \rightarrow CO_2 + 0.5\,N_2$	$A_4 = 1.18 \times 10^{19}$	$E_{a4} = 90000$

kinetic rate expressions presented originally by Voltz et al. [25] with modified kinetic constants and activation energies. The reaction scheme and the rate expressions used here are presented in Table B.1 and the reaction parameters in Table B.2. The inhibition terms used in the present study are those used by Tsinoglou et al. [43] for a similar TWC.

References

[1] H. Santos, M. Costa, The relative importance of external and internal transport phenomena in three way catalysts, International Journal of Heat and Mass Transfer 51 (2008) 1409–1422.

[2] P. Kočí, M. Kubíček, M. Marek, Modeling of three-way catalyst monolith converters with microkinetics and diffusion in the washcoat, Industrial Engineering Chemistry Research 43 (2004) 4503–4510.

[3] E. Massing, J.F. Brilhac, A. Brillard, P. Gilot, G. Prado, Modelling of the behaviour of a three way catalytic converter at steady state, Influence of the propene diffusion inside the catalytic layer, Chemical Engineering Science 55 (2000) 1707–1716.

[4] P. Kočí, F. Štěpánek, M. Kubíček, M. Marek, Meso-scale modelling of CO oxidation in digitally reconstructed porous Pt/γ-Al_2O_3 catalyst, Chemical Engineering Science 61 (2006) 3240–3249.

[5] K. Zygourakis, R. Aris, Multiple oxidation reactions and diffusion in the catalytic layer of monolith reactors, Chemical Engineering Science 38 (1983) 733–744.

[6] R. Wanker, H. Raupenstrauch, G. Staudinger, A fully distributed model for the simulation of a catalytic combustor, Chemical Engineering Science 55 (2000) 4709–4718.

[7] H. Santos, M. Costa, Evaluation of the conversion efficiency of ceramic and metallic three way catalytic converters, Energy Conversion and Management 49 (2008) 291–300.

[8] P. Avila, M. Montes, E. Miró, Monolithic reactors for environmental applications: a review on preparation technologies, Chemical Engineering Journal 109 (2005) 11–36.

[9] A.M. Holmgren, Enhanced mass transfer in monolith catalysts with bumps on the channels walls, Industrial Engineering Chemistry Research 38 (1999) 2091–2097.

[10] K.M. Haas, M. Rice, Innovative metallic substrates for exhaust emission challenges for gasoline and diesel engines, SAE Paper 2005-01-3851, 2005.

[11] S. Suárez, M. Yates, P. Avila, J. Blanco, New TiO_2 monolith supports based on the improvement of the porosity, Catalysis Today 105 (2005) 499–506.

[12] Z.Y. Yuan, B.L. Su, Insights into hierarchically meso-macroporous structured materials, Journal of Materials Chemistry 16 (2006) 663–677.

[13] S. Siemund, J.P. Leclerc, D. Schweich, M. Prigent, F. Castagna, Three-way monolith converter: simulations versus experiments, Chemical Engineering Science 51 (1996) 3709–3720.

[14] S. Tischer, Y. Jiang, K.W. Hughes, M.D. Patil, M. Murtagh, Three-way-catalyst modeling – a comparison of 1D and 2D simulations, SAE Paper, 2007-01-1071, 2007.

[15] K. Zygourakis, Transient operation of monolith catalytic converters: a two-dimensional reactor model and the effects of radially nonuniform flow distribution, Chemical Engineering Science 44 (1989) 2075–2086.

[16] L.L. Raja, R.J. Kee, O. Deutschmann, J. Warnatz, L.D. Schmidt, A critical evaluation of Navier-Stokes, boundary-layer, and plug-flow models of the flow and chemistry in a catalytic-combustion monolith, Catalysis Today 59 (2000) 47–60.

[17] G. Groppi, A. Belloli, E. Tronconi, P. Forzatti, A comparison of lumped and distributed models of monolith catalytic reactors, Chemical Engineering Science 50 (1995) 2705–2715.

[18] S.T. Lee, R. Aris, On the effects of radiative heat transfer in monoliths, Chemical Engineering Science 32 (1977) 827–837.

[19] C. Brinkmeier, Automotive three-way exhaust aftertreatment under transient conditions – measurements, modeling and simulation, PhD Thesis, Universität Stuttgart, Stuttgart, 2006.

[20] G. McCullough, R. Douglas, G. Cunnigham, L. Foley, The development of a two-dimensional transient catalyst model for direct injection two-stroke applications, Proceedings of the Institute of Mechanical Engineers Part D 215 (2001) 919–933.

[21] F. Zhang, R.E. Hayes, S.T. Kolaczkowski, A new technique to measure the effective diffusivity in the washcoat of a monolith reactor, Chemical Engineering Research and Design 82 (A4) (2004) 481–489.

[22] T. Starý, O. Šolcová, P. Schneider, M. Marek, Effective diffusivities and pore-transport characteristics of washcoated ceramic monolith for automotive catalytic converter, Chemical Engineering Science 61 (2006) 5934–5943.

[23] R. Holder, M. Bollig, D.R. Anderson, J.K. Hochmuth, A discussion on transport phenomena and three-way kinetics of monolithic converters, Chemical Engineering Science 61 (2006) 8010–8027.

[24] J.P. Day, Substrate effects on light-off – part I: thermal energy requirements, SAE Paper 962074, 1996.

[25] S.E. Voltz, C.R. Morgan, D. Liederman, S.M. Jacob, Kinetic study of carbon monoxide and propylene oxidation on platinum catalysts, Industrial Engineering Chemistry Production Research and Development 12 (1973) 294–301.

[26] D. Kryl, P. Kočí, M. Kubíček, M. Marek, T. Maunula, M. Härkönen, Catalytic converters for automobile diesel engines with adsorption of hydrocarbons on zeolites, Industrial Engineering Chemistry Research 44 (2005) 9524–9534.

[27] M. Votsmeier, J. Gieshoff, M. Kögel, M. Pfeifer, J.F. Knoth, A. Drochner, H. Vogel, Wall-flow filters with wall-integrated oxidation catalyst: a simulation study, Applied Catalysis B: Environmental 70 (2007) 233–240.

[28] Q. Xiao, B. Cheng, W.Q. Tao, Experimental study on effect of interwall tube cylinder on heat/mass transfer characteristics of corrugated plate fin-and-tube exchanger configuration, Journal Heat Transfer 114 (1992) 755–759.

[29] R.E. Hayes, S.T. Kolaczkowski, P.K.C. Li, S. Awdry, Evaluating the effective diffusivity of methane in the washcoat of a honeycomb monolith, Applied Catalysis B: Environmental 25 (2000) 93–104.

[30] S.T. Kolaczkowski, Measurement of effective diffusivity in catalyst-coated monoliths, Catalysis Today 83 (2003) 85–95.

[31] V. Balakotaiah, D.H. West, Shape normalization and analysis of the mass transfer controlled regime in catalytic monoliths, Chemical Engineering Science 57 (2002) 1269–1286.

[32] K. Ramanathan, V. Balakotaiah, D.H. West, Light-off criterion and transient analysis of catalytic monoliths, Chemical Engineering Science 58 (2003) 1381–1405.

[33] D. Leung, R.E. Hayes, S.T. Kolaczkowski, Diffusion limitation effects in the washcoat of a catalytic monolith reactor, The Canadian Journal of Chemical Engineering 74 (1996) 94–103.

[34] A. Nakhjavan, P. Björnbom, F.M. Zwinkels, S.G. Järas, Numerical analysis of the transient performance of high-temperature monolith catalytic combustors: effect of catalyst porosity, Chemical Engineering Science 50 (1995) 2255–2262.

[35] D. Papadias, L. Edsberg, P. Björnbom, Simplified method for effectiveness factor calculations in irregular geometries of washcoats, Chemical Engineering Science 55 (2000) 1447–1459.

[36] R. Aris, The Mathematical Theory of Diffusion and Reaction in Permeable Catalysts, vol. 1: The Theory of the Steady State, Clarendon Press, Oxford, 1975.

[37] R.E. Hayes, B. Liu, M. Votsmeier, Calculating effectiveness factors in non-uniform washcoat, Chemical Engineering Science 60 (2005) 2037–2050.

[38] R.E. Hayes, P.K. Mok, J. Mmbaga, M. Votsmeier, A fast approximation method for computing effectiveness factors with non-uniform kinetics, Chemical Engineering Science 62 (2007) 2209–2215.

[39] C. Depcik, D. Assanis, One-dimensional automotive catalyst modeling, Progress in Energy and Combustion Science 31 (2005) 308–369.

[40] G. Konstantas, Development and application of a computer aided engineering methodology supporting the design optimization of automotive exhaust treatment systems, PhD Thesis, Mechanical Engineering Department, University of Thessaly, Volos, 2006, http://www.mie.uth.gr/labs/ltte/grk/pubs/PhD_G_Konstantas.pdf.

[41] L. Olsson, B. Andersson, Kinetic modeling in automotive catalysis, Topics in Catalysis 28 (2004) 89–98.

[42] J.H.B.J. Hoebink, R.A. van Gemert, J.A.A. van den Tillaart, G.B. Marin, Competing reactions in three-way catalytic converters: modelling of NO_x conversion maximum in the light-off curves under net oxidising conditions, Chemical Engineering Science 55 (2000) 1573–1581.

[43] D.N. Tsinoglou, G.C. Koltsakis, J.C. Peyton Jones, Oxygen storage modeling in three-way catalytic converters, Industrial Engineering Chemistry Research 41 (2002) 1152–1165.